Online capacitance estimation of DC-link electrolytic capacitors for three-phase AC/DC/AC PWM converters using recursive least squares method

D.-C. Lee, K.-J. Lee, J.-K. Seok and J.-W. Choi

Abstract: A novel online capacitance estimation method for a DC-link capacitor in a three-phase AC/DC/AC PWM converter is prepared. At no load, a controlled AC current with a lower frequency than the line frequency is injected into the input side, which then causes AC voltage ripples at the DC output side. By extracting the AC voltage and current components on the DC output side using digital filters, the capacitance can then be calculated using the recursive least squares method. The proposed method can be simply implemented with only software and no additional hardware. Experimental results confirm that the estimation error is less than 0.26%.

1 Introduction

Three-phase AC/DC/AC PWM converters are being increasingly used for industrial applications, such as mill drives, elevators, wind power generation systems [1], UPQC (unified power quality conditioner) [2], and so on. The AC/DC/AC PWM converters usually have a DC-link consisting of electrolytic capacitor banks as an energy buffer. The lifetime of electrolytic capacitors is usually shorter than that of the other components of a power converter, and its capacitance decreases with aging. For example, the ratio of the electrolytic capacitor failure to the total failure of the DC/DC switch-mode power supply is 60% [3]. The lifetime of capacitors is normally considered to be over when the capacitance is reduced by more than 25% from the initial value [4]. Thus, determining the appropriate time to replace a capacitor is important for safe operation.

However, despite the importance of the electrolytic capacitor in power converters, related research work is limited. A deterioration diagnosis scheme of electrolytic capacitors in a forward-type converter and a buck-boost converter was proposed in [5]. This method utilises that the ESR (equivalent series resistance) of the capacitor increases as it deteriorates, and the ripple component varies in proportion to the ESR. Another failure prediction method of the capacitors for the switch-mode power supply was published in [6], where the ESR is estimated by processing the ripple voltage, by which the remaining time for failure is predicted. In [5] and [6], the fault of one capacitor cannot be predicted if several capacitors are in parallel. So, a smart electronic circuit was designed to indicate the failure of each capacitor in [3]. On the other hand, lifetime predictions of the capacitor from the initial time have been suggested [7, 8], yet the algorithms are complicated and precise estimation is difficult to achieve because the capacitor characteristics are sensitive to the operating frequency and temperature.

The DC-link capacitors used in the AC/DC/AC PWM converters are installed inside the system, making it difficult to measure the capacitance without detaching the capacitors, which is especially troublesome for wind power generation systems located offshore or on high towers.

Accordingly, to overcome these difficulties, this paper proposes a novel online capacitance estimation method for the AC/DC/AC PWM converter systems. To diagnose the degree of deterioration, the capacitance of the capacitor is periodically estimated using an input current injection and the RLS method. In an initial no-load condition, a particular AC current with a lower frequency than the power line frequency is injected into the input side of the AC/DC PWM converter. The output current of the AC/DC PWM converter then completely flows through the DC-link capacitor bank, as the load is virtually disconnected at the initial state. The injected input current causes an AC ripple voltage component in the DC output voltage that can be easily extracted from the measured voltage by using bandpass filters. Meanwhile, the DC-side current can be estimated from the AC input current and gating times of the switching devices, since it is not usually measured. As a result, the current and voltage information on the DC side can be used to calculated the capacitance based on the recursive least squares (RLS) method. When compared with the capacitance value measured by an LCR meter, it is confirmed that the estimation error is less than 0.26%. The experimental results for three-phase AC/DC/AC PWM converters also verify the effectiveness of the proposed algorithm.

2 Estimation of capacitance of DC-link capacitors

2.1 Current injection

Figure 1 shows a control block diagram of the three-phase AC/DC PWM converter(front-end converter) involving the blocks of the capacitance estimation algorithm. There are a DC-link voltage control loop and two current control loops. The AC phase current are transformed into the *d*- and

© IEE, 2005

IEE Proceedings online no. 20050027

doi:10.1049/ip-epa:20050027

Paper first received 28th January and in final revised form 3rd July 2005

D.-C. Lee and J.-K. Seok are with the Yeungnam University, 214-1, Daedong, Gyeongsan, Gyeongbuk, 712-749, Korea

K.-J. Lee is with Inverter Part, LG Philips LCD, Gumi, Gyeongbuk, Korea

J.-W. Choi is with the Kyungpook National University, 1370, Sankyuk-Dong, Buk-Gu, Daegu, Korea

E-mail: dclee@yu.ac.kr

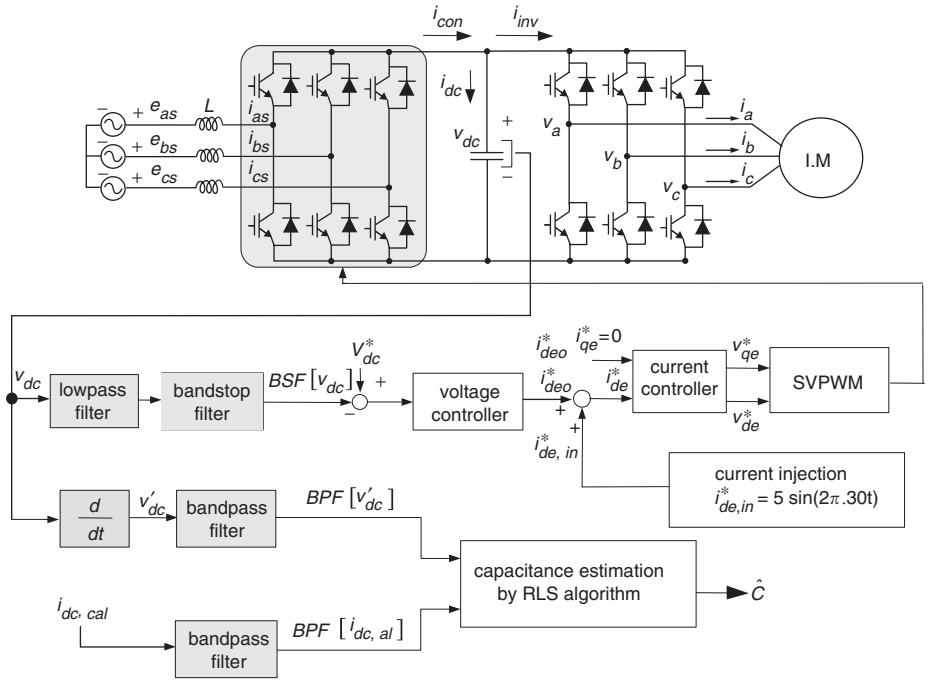

Fig. 1 *Block diagram for estimating DC capacitance for three-phase PWM converters*

q-axis currents in a synchronous reference frame. The q-axis current is controlled at zero for a unity power factor operation on the source side, whereas the d-axis current is controlled to keep the DC voltage constant.

Let us consider the operation of an AC/DC/AC PWM converter under no-load condition, which means that the inverter side is virtually disconnected from the DC-link. If the DC output voltage is well controlled at its reference value, the d-axis current reference, which is a real power component, is zero and the DC-link voltage is kept constant, except for the switching frequency-related ripple components. However, since this is an equilibrium state, it is difficult to obtain any information on the system parameters from this condition. Thus, a specific signal needs to be injected to excite the system, for example, a regulated AC current with a low frequency can be injected into the input side of the AC/DC PWM converter. In Fig. 1, the injected current reference in the synchronous reference frame is given as

$$i^*_{de,in} = 5\sin(2\pi \times 30t) \tag{1}$$

When $i_{de,in}$ is well controlled and is inversely transformed into the stationary reference frame, the AC current of the pulsed waveform with a fundamental frequency of 30 Hz flows through the line and the DC-link capacitors. This current causes a ripple voltage at the same frequency. The AC current and voltage are used to determine the capacitance based on the RLS method.

The lower the frequency of the injected current with the same magnitude, the larger the magnitude of the ripple voltage. Thus, a lower frequency AC current is preferable to obtain a ripple voltage with a significant magnitude, since the allowable ripple current level of the capacitor is not so high [9].

2.2 DC link current

To calculate the capacitance, the capacitor current needs to be known. While the AC line currents are often measured for current control and overcurrent protection, the DC-link current is rarely measured for this purpose. Thus, instead of a direct measurement, the DC-link current (i_{dc}) can be reconstructed from the AC input currents (i_{as}, i_{bs}, i_{cs}) and switching functions (S_a, S_b, S_c) as in [10, 11]:

$$i_{dc} = S_a i_{as} + S_b i_{bs} + S_c i_{cs} \tag{2}$$

where the switching function is '1' or '0' when an upper switch of each switching pole turns on or off, respectively.

Since the instantaneous current of the capacitor in (2) is a pulsed waveform, it is difficult to obtain the fundamental component. Thus, after eliminating the high-frequency component using a lowpass filter, the AC component at the frequency of the injected current can be extracted using a bandpass filter. However, this process is complicated. Therefore, if the gating time and phase currents are used, the mean value of the DC-link current, $i_{dc,cal}$, at each sampling period can be found as

$$i_{dc,cal} = (T_{ga} i_{as} + T_{gb} i_{bs} + T_{gc} i_{cs})/T_{samp} \tag{3}$$

where T_{ga}, T_{gb} and T_{gc} are the gating time for each phase and T_{samp} is the sampling period.

Figure 2 shows the relationship between the phase current and the DC-link current according to the switching state, where A^+, B^+ and C^+ represent the gating signals for upper switches of each switching pole. It is shown that the instantaneous DC-link current waveforms can be reconstructed with the phase currents and the gating signals. The waveform of $i_{dc,cal}$ shows a natural filtering effect of instantaneous DC-link currents of i_{dc}. If the dead time effect of the switching devices is compensated well, its influence on calculation of (3) can be ignored [12].

2.3 Digital filtering

To extract the AC components from the derivative of the measured DC voltage and the calculated DC-link current in (3), a second-order bandpass filter is used [13, 14], and the transfer function is given by

$$H_{BPF}(s) = \frac{K_{BPF}(\omega_{BPF}/Q_{BPF})s}{s^2 + (\omega_{BPF}/Q_{BPF})s + \omega^2_{BPF}} \tag{4}$$

where K_{BPF} is the gain, Q_{BPF} is the quality factor, f_{BPF} is the cutoff frequency, and $\omega_{BPF} = 2\pi f_{BPF}$. The filter output characteristic is not so sensitive to the quality factor because

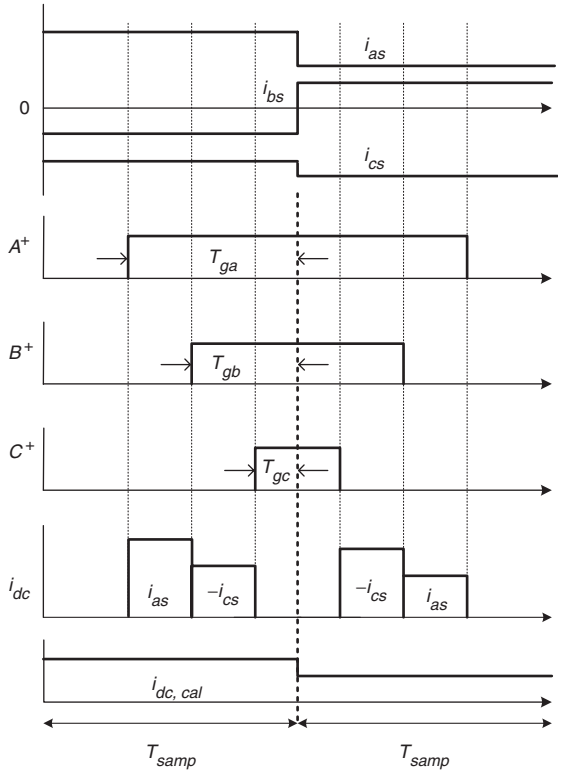

Fig. 2 *Instantaneous and averaged DC-link currents according to gating pulses and phase currents*

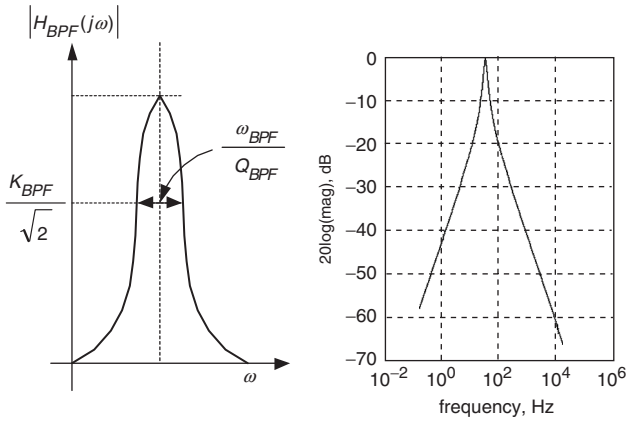

Fig. 3 *Gain curve of bandpass filter*

there is no other component near 30 Hz frequency. Figure 3 shows the frequency response of the bandpass filter when $K_{BPF}=1$, $Q_{BPF}=4$ and $f_{BPF}=30$ Hz.

Meanwhile, the AC ripple voltage component needs to be rejected since the mean value of the DC-link voltage should be fed back to control the DC voltage. Thus, a second-order bandstop filter is used, and the transfer function is given by

$$H_{BSF}(s)=\frac{K_{BSF}(s^2+\omega_{BSF}^2)}{s^2+(\omega_{BSF}/Q_{BSF})s+\omega_{BSF}^2} \tag{5}$$

where K_{BSF} is the gain, Q_{BSF} is the quality factor, f_{BSF} is the cutoff frequency, and $\omega_{BSF}=2\pi f_{BSF}$. Figure 4 shows the frequency response of the bandstop filter when $K_{BSF}=1$, $Q_{BSF}=2$ and $f_{BSF}=30$ Hz, where the selection of Q_{BSF} is not so sensitive either.

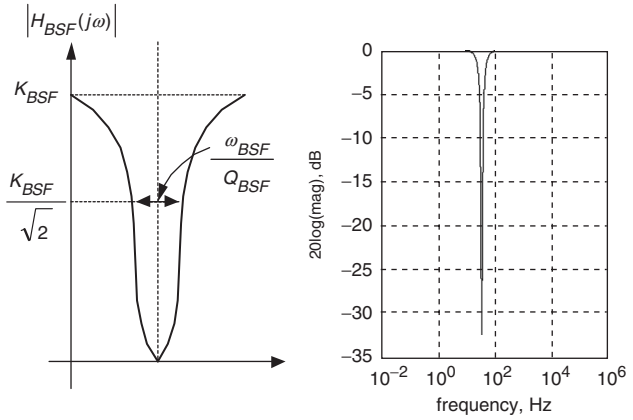

Fig. 4 *Gain curve of bandstop filter*

The voltage filtered by the bandpass filter still contains the high-frequency components due to the switching action of the devices. Thus, to eliminate these components, a second-order lowpass filter is used at the front-end of the bandstop filter, and transfer function is given by

$$H_{LPF}(s)=\frac{K_{LPF}\omega_{LPF}^2}{s^2+(\omega_{LPF}/Q_{LPF})s+\omega_{LPF}^2} \tag{6}$$

where $K_{LPF}=1$, $Q_{LPF}=2$, $f_{LPF}=200$ Hz and $\omega_{LPF}=2\pi f_{LPF}$ were chosen for the experiments.

2.4 Recursive least squares method

The capacitance of a DC-link capacitor bank can be estimated using the injected current and output voltage, where the relation between the current and the voltage of the capacitor is given by

$$i_{dc}=C\frac{dv_{dc}}{dt}=Cv'_{dc} \tag{7}$$

To extract only the required AC components of the current and voltage, the bandpass filters are applied to both sides in (7), as explained previously, which gives

$$BPF[i_{dc}]=C\times BPF[v'_{dc}] \tag{8}$$

where '$BPF[\cdot]$' represents the bandpass filtered quantity. Then, the unknown parameter, the capacitance, can be easily estimated using an RLS algorithm [15, 16].

The RLS algorithm iteratively minimises the least square cost function, allowing the estimated parameter of the system to be updated at each sample interval whenever new data become available. The RLS identification algorithm has the advantages of simple calculation and good convergence properties against other methods, thus it is one of the preferred techniques used for system parameter identification.

Next, consider the error criterion. The error cost function is expressed as

$$e^2(n)=\left[BPF[i_{dc}(n)]-\hat{C}(n)BPF[v'_{dc}(n)]\right]^2 \tag{9}$$

where $\hat{C}$ is the estimated value of the capacitance. The gradient of the error with respect to $\hat{C}(n)$ is given by

$$\frac{\partial e^2(n)}{\partial\hat{C}(n)}=-2BPF[v'_{dc}(n)]\left[BPF[i_{dc}(n)]-\hat{C}(n)BPF[v'_{dc}(n)]\right] \tag{10}$$

which means that the parameter $\hat{C}(n)$ should be updated so that the right-side terms in (10) can minimise the error cost function $e^2(n)$. So, the RLS update of the parameter $\hat{C}(n)$

can be written

$$\hat{C}(n+1) = \hat{C}(n) + \gamma(n)BPF[v'_{dc}(n)] \times \left[BPF[i_{dc}(n)] - \hat{C}(n)BPF[v'_{dc}(n)]\right] \quad (11)$$

where $\gamma(n)$ is an adjustment gain and was selected as a constant scalar gain ($=9.5\times10^{-8}$) in the experiment by a trial and error method. The initial value of $\hat{C}(0)$ can be either the estimated capacitance from the last capacitor diagnosis or the nominal value of the capacitor bank.

3 Experimental results

To verify the effectiveness of the proposed scheme, experiments were carried out using the setup shown in Fig. 5 and Table 1. The TMS320C31 DSP chip operating at 33.3 MHz is used as a main processor and the power capacity of the AC/DC/AC PWM converter using IGBT modules is 3 kVA. In fact, this type of power converter is usually used for AC machine drives higher than medium power level. The input inductor is needed for boosting action of the voltage. The capacitances of the capacitors used for the experiment were measured by the HIOKI 3532 LCR meter, which has an instrument accuracy of $\pm0.08\%$. The measured capacitances are lower than the nominal values due to the aging effect of the capacitor at the laboratory.

Even though the three-phase AC/DC/AC PWM converters are prepared for induction motor drives, only the source-side AC/DC PWM converter is operated for the capacitor bank diagnosis, while the PWM inverter is at idle condition. When the capacitance estimation algorithm begins, $i^*_{de,in} = 5\sin(2\pi\times30t)$ is given for the d-axis current

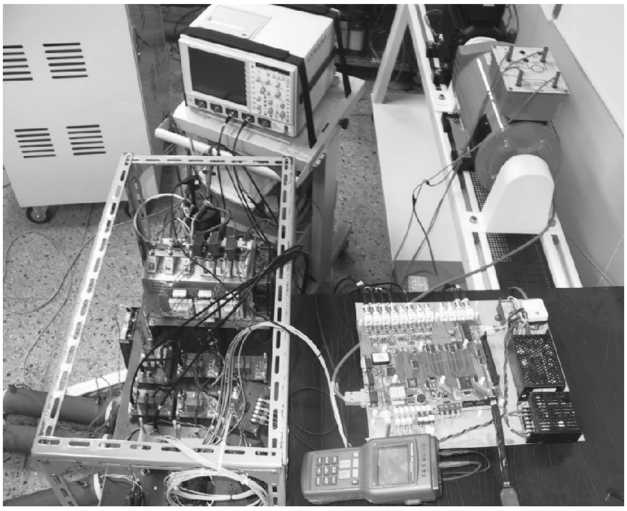

Fig. 5 *Experimental setup*

Table 1: System parameters

Input voltage	Three-phase 220 V	
Input boost inductance	3.5 mH	
Line resistance	0.5 Ω	
Converter capacity	3 kVA	
Switching frequency	3.5 kHz	
Injected current	5 Apk, 30 Hz	
DC-link voltage	350 V	
Capacitor	Nominal capacitance	Measured ones
	$C_1 = 3300\,\mu F$	$C_1 = 3105\,\mu F$
	$C_2 = 2350\,\mu F$	$C_2 = 2180\,\mu F$
	$C_3 = 500\,\mu F$	$C_3 = 469\,\mu F$

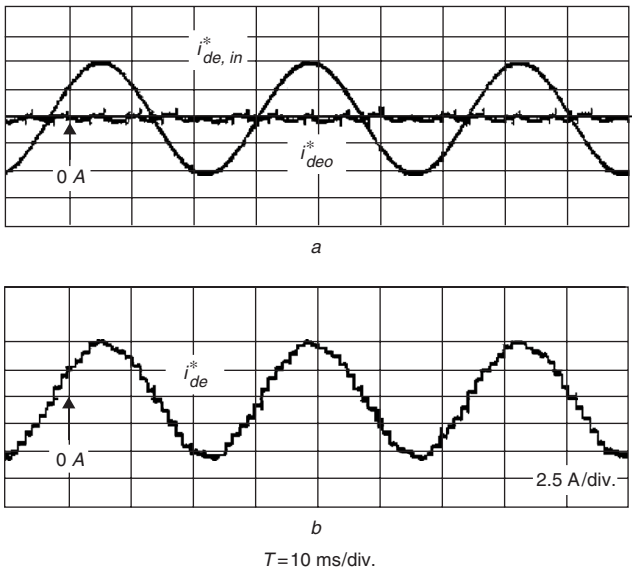

Fig. 6 *Voltage controller output and injected current*

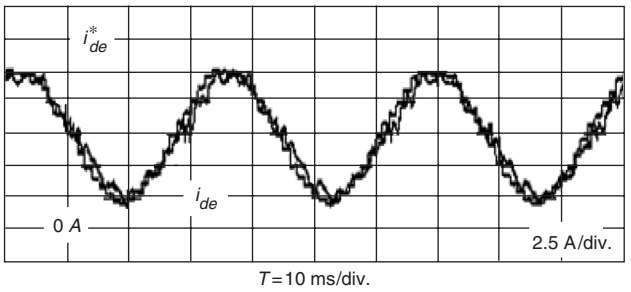

Fig. 7 *D-axis current and its reference*

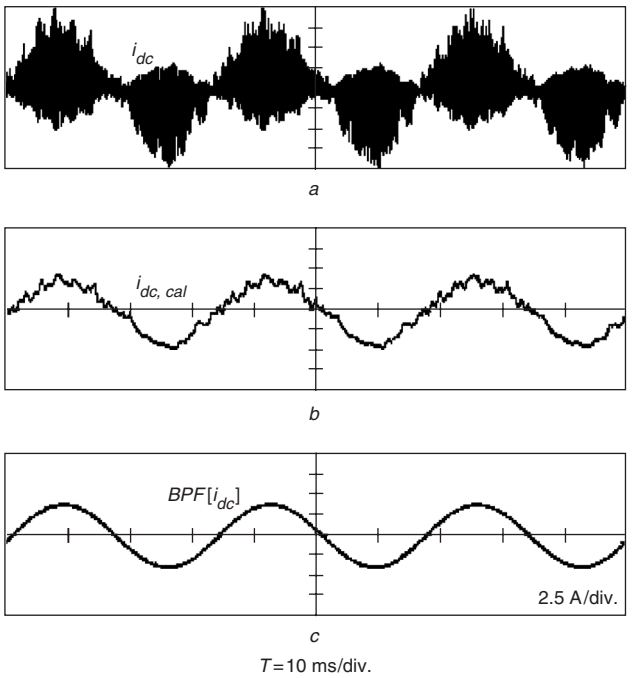

Fig. 8 *DC-link currents*
a Measured
b Calculated
c Bandpass filtered

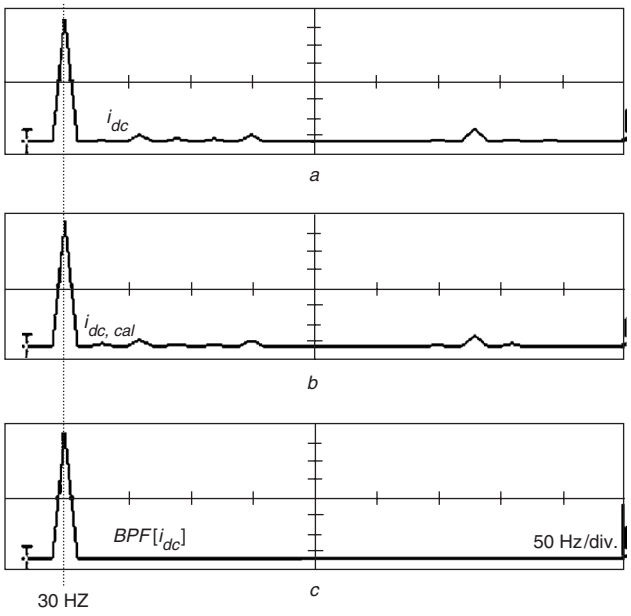

Fig. 9 *Harmonic spectrum of DC-link currents*
a Measured
b Calculated
c Bandpass filtered

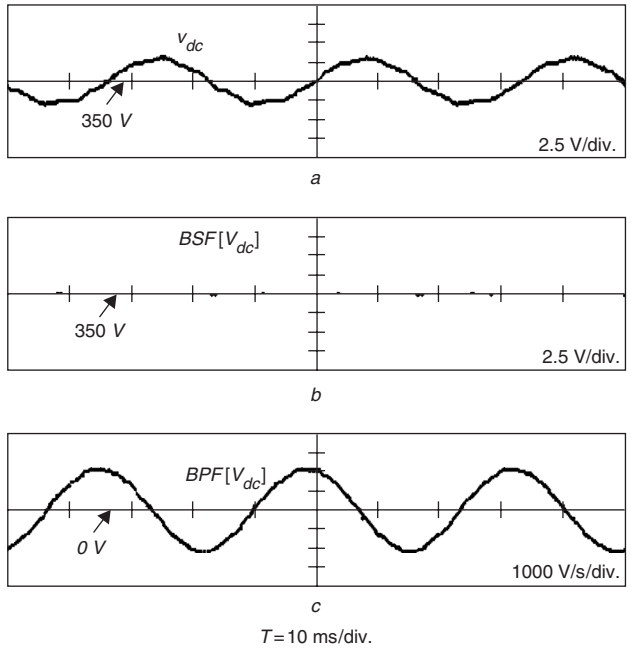

Fig. 10 *DC-link voltages*
a Measured
b Bandstop filtered
c Bandpass filtered (of derivative)

reference and $i^*_{qe} = 0$ for the q-axis current reference for a unity power factor operation. The DC-link voltage is controlled as 350 V.

Figure 6*a* shows the voltage controller output i^*_{de0} at no load and injected d-axis current reference $i^*_{de,in}$, and Fig. 6*b* shows the modified reference i^*_{de} obtained by adding these two references. Since the q-axis current is controlled at zero for a unity power factor, the voltage controller output, i^*_{de0}, is also maintained at zero for no load. Thus, i^*_{de} is equal to $i^*_{de,in}$. Figure 7 shows the d-axis current control performance. The AC component is also well controlled.

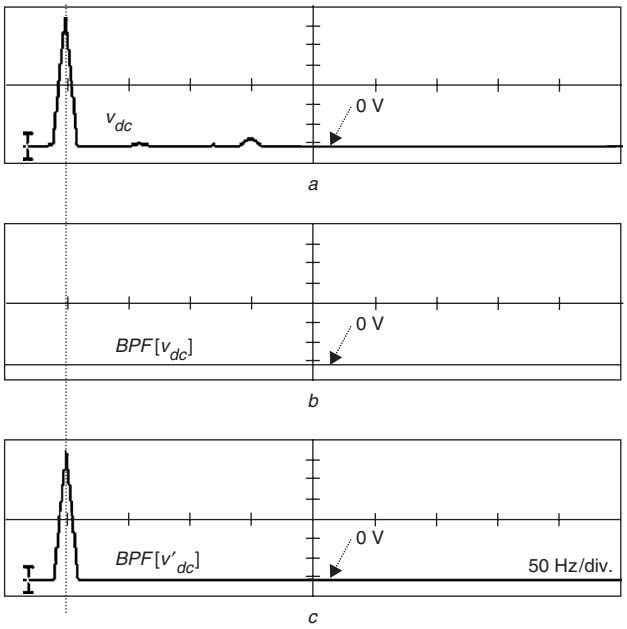

Fig. 11 *Harmonic spectrum of DC-link voltages*
a Measured
b Bandstop filtered
c Bandpass filtered

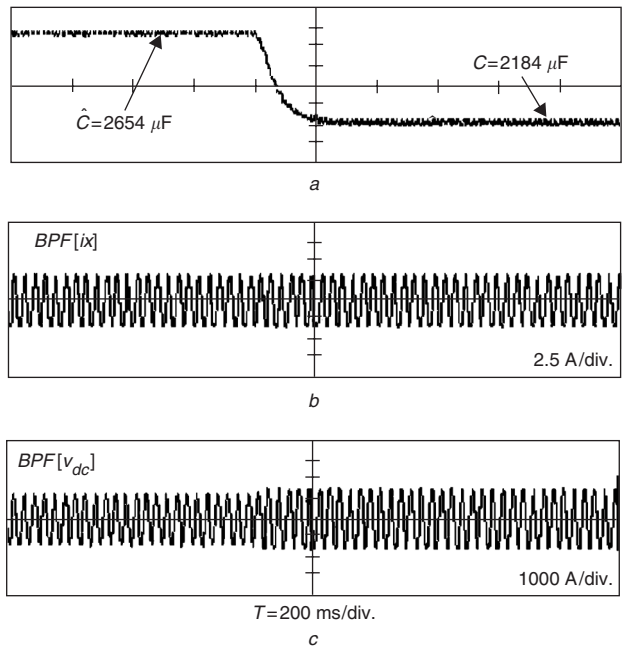

Fig. 12 *Capacitance estimation at abrupt variation of C*

Table 2: Measured and estimated capacitances

Measured capacitance, μF	Estimated capacitance, μF	Estimation error
3105	3107	+0.064%
2650	2654	+0.15%
2180	2184	+0.18%

Figure 8 shows the DC-link currents, where Fig. 8*a* is the DC current measured directly by a current probe, Fig. 8*b* is the waveform reconstructed by (3), and Fig. 8*c* is the bandpass-filtered waveform from the waveform in Fig. 8*b*.

Figure 9 shows the harmonic spectrum of the DC-link currents corresponding to Fig. 8. Clearly, the other frequency components, except for the 30 Hz component, are completely eliminated after applying the BPF.

Figure 10 shows the DC output voltages, where Fig. 10*a* is the measured waveform, Fig. 10*b* is the bandstop-filtered waveform for voltage feedback control, and Fig. 10*c* is the bandpass-filtered waveform from the derivative of Fig. 10*b*. Figure 11 shows the harmonic spectrum of the DC ripple voltage corresponding to Fig. 10. The performance of the filters is very satisfactory.

Figure 12 shows the variation in the estimated capacitance value, DC-link ripple voltage, and current when C_3 is abruptly opened while C_2 and C_3 are being connected in parallel. Even though the capacitance value changes abruptly, it is still well estimated.

Table 2 shows a list of the estimated and measured data for the different capacitors tested. The estimation errors in all cases are less than 0.26% including the instrument accuracy of $\pm 0.08\%$.

4 Conclusions

This paper has presented and implemented a novel online capacitance estimation method for a three-phase AC/DC/AC PWM converter. The proposed scheme does not require any extra hardware, but is rather executed using software, based on injecting an AC input current, processing the current and voltage signals with digital filters, and using the RLS method. Experimental results confirmed that the capacitance estimation error was less than 0.26%, making the proposed algorithm very effective for diagnosing the deterioration of DC electrolytic capacitor banks in the AC/DC/AC PWM converter system.

5 References

1 Pena, R., Clare, J., and Asher, G.M.: 'Doubly fed induction generator using back-to-back pwm converters and its application to variable-speed wind-energy generation', *IEE Proc., Electr. Power Appl.*, 1996, **143**, (3), pp. 231–241

2 Fujita, H., and Akagi, H.: 'The unified power quality conditioner: the integration of series- and shunt-active filters', *IEEE Trans. Power Electron.*, 1998, **13**, (2), pp. 315–322

3 Venet, P., Perisse, F., El-Husseini, M.H., and Rojat, G.: 'Realization of a smart electrolytic capacitor circuit', *IEEE Ind. Appl. Mag.*, 2002, **8**, (1), pp. 16–20

4 Hitachi AIC Inc., 'Estimated life of aluminium electrolytic capacitors', Tokyo, Japan, 1999

5 Harada, K., Katsuki, A., and Fujiwara, M.: 'Use of esr for deterioration diagnosis of electrolytic capacitor', *IEEE Trans. Power Electron.*, 1993, **8**, (4), pp. 355–361

6 Lahyani, A., Venet, P., Grellet, G., and Viverge, P.-J.: 'Failure prediction of electrolytic capacitors during operation of a switchmode power supply', *IEEE Trans. Power Electron.*, 1998, **13**, (6), pp. 1199–1207

7 Gasperi, M.L.: 'A method for predicting the expected life of bus capacitor'. Proc. IEEE IAS Conf., 1997, pp. 1042–1047

8 Lee, D.-C., and Kim, H.-J.: 'Life estimation of electrolytic capacitors for inverters', *Trans. Korean Inst. Electr. Eng.*, 2001, **50B**, (7), pp. 338–346

9 Hayatee, F.G.: 'Heat dissipation and ripple current rating in electric capacitors', *Electrocompon. Sci. Tech.*, 1975, **2**, pp. 109–114

10 Blaabjerg, F., Pedersen, J.K., Jaeger, U., and Thoegersen, P.: 'Single current sensor technique in the dc link of three-phase pwm-vs inverters: a review and a novel solution', *IEEE Trans. Ind. Appl.*, 1997, **33**, (5), pp. 1241–1253

11 Lee, D.-C., and Lim, D.-S.: 'AC voltage and current sensorless control of three-phase pwm rectifiers', *IEEE Trans. Power Electron.*, 2002, **17**, (6), pp. 883–890

12 Choi, J.-W., and Sul, S.-K.: 'Inverter output voltage synthesis using novel dead time compensation', *IEEE Trans. Power Electron.*, 1996, **11**, (2), pp. 221–227

13 Chassaing, R.: 'Digital signal processing' (John Wiley & Sons Inc., 1999)

14 McClellan, J.H., Schafer, R.W., and Yoder, M.A.: 'Dsp first' (Prentice Hall, 1999)

15 Haykin, S., and Widrow, B.: 'Least-mean-square adaptive filters' (Wiley Publishing, 2003)

16 Wellstead, P.E., and Zarrop, M.B.: 'Self-tuning systems: control and signal processing' (John Wiley & Sons, 1991)